*Retraction*

# Retracted: Robotic Arm Control System Based on AI Wearable Acceleration Sensor

## Mathematical Problems in Engineering

This article has been retracted by Hindawi following an investigation undertaken by the publisher [1]. This investigation has uncovered evidence of one or more of the following indicators of systematic manipulation of the publication process:

(1) Discrepancies in scope

(2) Discrepancies in the description of the research reported

(3) Discrepancies between the availability of data and the research described

(4) Inappropriate citations

(5) Incoherent, meaningless and/or irrelevant content included in the article

(6) Peer-review manipulation

The presence of these indicators undermines our confidence in the integrity of the article's content and we cannot, therefore, vouch for its reliability. Please note that this notice is intended solely to alert readers that the content of this article is unreliable. We have not investigated whether authors were aware of or involved in the systematic manipulation of the publication process.

Wiley and Hindawi regrets that the usual quality checks did not identify these issues before publication and have since put additional measures in place to safeguard research integrity.

We wish to credit our own Research Integrity and Research Publishing teams and anonymous and named external researchers and research integrity experts for contributing to this investigation.

The corresponding author, as the representative of all authors, has been given the opportunity to register their agreement or disagreement to this retraction. We have kept a record of any response received.

## References

[1] L. Chen, H. Sun, W. Zhao, and T. Yu, "Robotic Arm Control System Based on AI Wearable Acceleration Sensor," *Mathematical Problems in Engineering*, vol. 2021, Article ID 5544375, 13 pages, 2021.

*Research Article*

# Robotic Arm Control System Based on AI Wearable Acceleration Sensor

**Liang Chen [ID],[1] Hanxu Sun,[1] Wei Zhao,[2] and Tao Yu[3]**

[1]*School of Automation, Beijing University of Posts and Telecommunications, Beijing 100876, China*
[2]*School of Information Engineering, Beijing Institute of Graphic Communications, Beijing, China*
[3]*College of Mechanical Engineering and Automation, Liaoning University of Technology, Jinzhou, Liaoning, China*

Correspondence should be addressed to Liang Chen; chenliang968@bupt.edu.cn

The position of mechanical arm in people's life is getting higher and higher. It replaces the function of human arm, moving and moving in space. Generally, the structure is composed of mechanical body, controller, servo mechanism, and sensor, and some specified actions are set to complete according to the actual production requirements. The manipulator has flexible operation, good stability, and high safety, so it is widely used in industrial automation production line. With the development of science and technology, many practical production requirements for the function of the manipulator are more and more refined, especially in the high-end research field. For example, medical devices, automobile manufacturing, deep-sea submarines, and space station maintenance put forward higher requirements for it. In terms of miniaturization and precision, it can meet the needs of scientific research and actual production. But these are inseparable from the motion control system technology. This paper mainly introduces the research of manipulator control system based on AI wearable acceleration sensor, aiming to provide some ideas and directions for the research of wearable manipulator. This paper presents the research method of manipulator control system based on AI wearable acceleration sensor, including the establishment of manipulator kinematics model, common filtering algorithm, and PI algorithm of speed control system. It is used for the research and experiment of manipulator control system based on AI wearable acceleration sensor. The experimental results show that the average matching rate of the manipulator control system based on AI wearable acceleration sensor is as high as 88.89%, and the stability of the feature descriptor is high.

## 1. Introduction

With the upgrading of modern sensors and microprocessors, robotics has developed rapidly. In the context of the era of artificial intelligence and the Internet of things, more intelligent robots have more room for development and have more applications in aviation exploration, deep-sea operations, medical assistance, smart homes, and automated factories. In the "Made in China 2025" strategic document, robotics is listed as one of the ten major development areas, which is enough to reflect the importance of the development of robotics in current life and production. As the most intuitive operation unit in the robot system, the robotic arm has become one of the most concerned research directions in the robotics research field under the increasingly stringent automation standards. How to make the control method of

the robotic arm more effective and convenient is currently the research hotspot. At present, most manipulators are roughly divided into two types according to the control method. The first is a dedicated manipulator that can complete preprogrammed processing actions by itself. Most of these control methods are industrial manipulators, which are often used in assembly lines in factories. It can be used to handle a lot of repetitive work; the second is a general-purpose manipulator that uses real-time command input manually to obtain the feedback action of the manipulator. The manipulator using this control method has high flexibility and can be used in tasks with complex environments.

The robotic arm is one of the most widely used automation devices in the field of robotics science and technology. At present, the traditional manipulator control methods are mostly completed by preprogramming

processing or command input from external devices. Such control methods are usually complicated and cumbersome and require operators to familiarize themselves with specific programming methods or according to different types of manipulators control instruction. With the advent of accelerometers, a brand-new noncontact somatosensory technology has been rapidly developed, showing a broad application prospect in the field of intelligent robots. In order to realize a more convenient and flexible manipulator control method, this paper designs a manipulator control system based on AI wearable acceleration sensor. The design of the robotic arm system better recognizes and senses changes in the human body, so as to achieve noncontact control.

Jarrahi's research found that artificial intelligence has penetrated into many organizational processes, leading to growing concerns that intelligent machines will soon replace humans in making decisions. In order to provide a more positive and pragmatic perspective, Jarrahi's research emphasizes the complementarity of humans and artificial intelligence and explores how to play their respective advantages in the organizational decision-making process, which is usually uncertain, complex, and ambiguous. Artificial intelligence has greater computational information processing capabilities and analysis methods, which can expand human cognition when dealing with complex problems, and humans can still provide a more comprehensive solution when dealing with uncertainties and ambiguities in organizational decisions intuitive method. This premise reflects the idea of intelligent enhancement, that is, the design of artificial intelligence systems should focus on enhancing rather than replacing human contributions. This research is theoretically strong, but lacks practical examples [1]. Choi and Kang proposed a software architecture of a wearable vital sign measurement device based on real-time user behavior recognition. Using wearable devices to measure vital signs helps users measure their health status related to their behavior, because wearable devices can be worn in daily life. Especially when the user is running or sleeping, blood oxygen saturation and heart rate are used to diagnose respiratory problems. However, in the measurement of vital signs, the traditional continuous measurement method is unreasonable because motion artifacts can reduce the accuracy of the vital signs. Moreover, due to the limited resources of wearable devices, in order to repair the distortion, Choi and Kang proposed a wearable device software architecture, which uses a simple filter and acceleration sensor to identify the user's behavior and measures accurately through the behavior state vital signs. This research lacks experimental data support and is not very scientific [2]. Navarro-Alarcon et al. proposed a feedback method that uses a manipulator to automatically servo control the three-dimensional shape of a soft object. Due to its potential applications in the food industry, household robots, medical robots, and manufacturing industries, the problem of soft object manipulation has attracted widespread attention from robotics researchers in recent years. A major complication in automatically controlling the shape

of an object is the estimation of its deformation characteristics, which determines how the motion of the manipulator is actively transformed into deformation. In order to solve this problem, Navarro-Alarcon et al. have developed a new algorithm for real-time calculation of soft object deformation parameters, which provides valuable adaptive behavior for deformation controllers, which cannot be achieved by traditional fixed model methods. In order to verify the proposed adaptive controller, a detailed experimental study of the robot was carried out. This research is not practical and not suitable for popularization in practice [3].

The innovations of this paper are as follows: (1) the commonly used filter processing algorithm is proposed for the research of the robotic arm control system based on the AI wearable acceleration sensor; (2) the PI algorithm of the speed control system is proposed for the AI wearable acceleration sensor; (3) based on the research on the arm control system, a wearable robotic arm that can be grasped collaboratively is designed.

## 2. Method of Robotic Arm Control System Based on AI Wearable Acceleration Sensor

*2.1. Establishment of Kinematic Model of Robotic Arm.* The size of the working space of the robotic arm reflects the kinematics of the robotic arm, and the kinematics of the robotic arm is the basis for the study of the working space of the robotic arm [4]. In order to accurately control the robot arm to complete the command action in the follow-up somatosensory control experiment, it is necessary to analyze the kinematics and workspace of the robot arm used in the experiment [5].

The D-H method is a robot attitude representation method described by Denavit and Hartenberg in the calculation of robot motion parameters. By establishing the corresponding coordinate system on each joint link and using the homogeneous transformation of the matrix, the position and posture relationship between adjacent links can be determined, and a series of coordinate systems can be transformed by matrix, so as to establish the robot arm kinematic model [6]. Use the DH method to determine the motion model of the robotic arm, where $a_i$ is the length of the link, $\theta_i$ is the angle between two adjacent joint axes, $d_i$ is the spatial distance between two adjacent links, and $\beta_i$ is the spatial angle of two adjacent links [7].

In order to determine the posture state of the operating end of the manipulator, the movement of each joint can be recursively step by step through the adjacent links [8]. The movement transfer process has the following matrix transformation formula:

$$
{}_{i}^{i-1}T = \begin{bmatrix} c\beta_i & -s\beta_i & 0 & a_{i-1} \\ s\beta_i c\theta_{i-1} & c\beta_i c\theta_{i-1} & -s\theta_{i-1} & -d_i s\theta_{i-1} \\ s\beta_i s\theta_{i-1} & c\beta_i s\theta_{i-1} & c\theta_{i-1} & d_i c\theta_{i-1} \\ 0 & 0 & 0 & 1 \end{bmatrix}. \tag{1}
$$

The transformation matrix between adjacent units is as follows:

$$
{}_1^0T = \begin{bmatrix} c\beta_1 & -s\beta_1 & 0 & 0 \\ s\beta_1 & c\beta_1 & 0 & 0 \\ 0 & 0 & 1 & 0 \\ 0 & 0 & 0 & 1 \end{bmatrix}, \tag{2}
$$

$$
{}_2^1T = \begin{bmatrix} c\beta_2 & -s\beta_2 & 0 & 0 \\ 0 & 0 & 1 & d_2 \\ -s\beta_2 & -c\beta_2 & 0 & 0 \\ 0 & 0 & 0 & 1 \end{bmatrix}, \tag{3}
$$

$$
{}_3^2T = \begin{bmatrix} c\beta_3 & -s\beta_3 & 0 & a_2 \\ s\beta_3 & c\beta_3 & 0 & 0 \\ 0 & 0 & 1 & 0 \\ 0 & 0 & 0 & 1 \end{bmatrix}. \tag{4}
$$

In order to manipulate the position vector between the end coordinate system reference and the base origin coordinate system, the following formula exists:

$$
P = \begin{bmatrix} a_3c_{23}c_1 - d_2s_1 + a_2c_1c_2 - d_1s_{234}c_1 \\ d_5\left(c_4\left(c_2s_1s_3 + c_3s_1s_2\right) - s_4\left(s_1s_2s_3 - c_2c_3s_1\right)\right) - a_3\left(s_1s_2s_3 - c_2c_3s_1\right) + a_2c_1s_1 \\ -a_3s_{23} - a_2s_2 - d_5c_{234} \end{bmatrix}. \tag{5}
$$

## 2.2. Common Filter Processing Algorithms.

Digital filtering methods are very commonly used in processing data noise. According to the different requirements of data processing in actual projects, the corresponding digital filtering methods can be selected [8, 9]. The different use characteristics of digital filtering can be divided into two categories: digital filtering methods that deal with occasional large interference and digital filtering methods that deal with small fluctuations in high frequency [10].

### 2.2.1. Digital Filtering Method to Deal with Occasional Large Interference.

During data acquisition, due to the unstable influence of the instrument, random and large interference sometimes occurs. This kind of data interference occurs at a low frequency, but it causes a great disturbance to the data analysis. For this kind of interference, limit filtering methods and median filtering methods can be used [11].

*(1) Limiting Filtering Method.* The principle of the limiting filtering method is to set a deviation threshold T based on actual projects and empirical judgments. When the detected two adjacent data exceed this threshold, the current measurement value is discarded and the previous measurement data is selected to replace [12, 13]. This filtering method can effectively remove random interference caused by accidental factors, but it cannot be used in data smoothness processing [14]. Its expression is

$$
\begin{cases} \left|Y\left(t_2\right) - Y\left(t_1\right)\right| \le T, Y\left(t_2\right) = Y\left(t_2\right), \\ \left|Y\left(t_2\right) - Y\left(t_1\right)\right| > T, Y\left(t_2\right) = Y\left(t_1\right). \end{cases} \tag{6}
$$

*(2) Median Filtering Method.* The median filter is a typical low-pass filter proposed by Yüzer et al. [15]. This technology can usually overcome the blurring of some details in the image generated by the linear filter under certain conditions and can eliminate the interference pulse well and at the same time can form a certain degree of protection for the edge of the target image [16].

The basic principle of median filtering is to establish a sliding window, which contains many pixels, and take the median value of all these pixels and use it as the new value of the center point of the window [17]. The specific process is to first determine a square (circular, diamond, linear, etc.) area with a certain pixel as the center. This neighborhood is generally called a window. Secondly, the gray values of all pixels in the window are sorted, and after sorting is completed, the median value in the arrangement is taken as the new value of the gray value of the center pixel of this window [18]. It should be noted here that if the number of pixels is odd, then the median value is the middle value after sorting by size; if the number of pixels is even, then the gray values of the middle two pixels after sorting are averaged as the middle value [19]. In the image denoising process, the image signal can be regarded as a two-dimensional signal, so the output of the median filter in the two-dimensional case can be expressed as

$$
g(x, y) = \text{median}\{f(x - i, y - j)\}, \quad (i, j) \in W, \tag{7}
$$

where $g(x, y)$ represents the gray value of the output pixel, $f(x - i, y - j)$ represents the input gray value, and $W$ is the template window [20].

### 2.2.2. Digital Filtering Method to Deal with Small Fluctuations in High Frequency.

For high-frequency and small-amplitude data fluctuations, the average filtering method is often used, which is characterized by the ability to suppress continuous small noise and high signal smoothness [21].

*(1) Arithmetic Average Filtering Method.* Arithmetic average filtering is to find the average value after summing the data of N consecutive samples. The following formula exists:

$$y = \frac{1}{N} \sum_{i=1}^{n} X_i. \qquad (8)$$

It can be seen that as $N$ increases, the result is more accurate, and the smoothness of the data after the solution increases, but the calculation time increases and the sensitivity decreases [22]. In actual engineering, the value of $N$ is usually selected according to specific requirements to obtain the required filtering effect [23].

*(2) Moving Average Filtering Method.* Arithmetic average filtering needs to collect N continuous data when determining the sampling value. This method has a slower detection time and is not suitable for high-frequency data input [24]. Moving average filtering is suitable for high-frequency input systems. First determine the window size. When there are new data, discard the first data in the window, fill the new data to the end of the window, and perform arithmetic average calculation on several fixed data in the window [25]. The following formula exists:

$$y(n) = \frac{1}{\text{windowSize}} (x(n) + x(n-1) + \cdots + x(n - (\text{windowSize} - 1))). \qquad (9)$$

*(3) Limiting Moving Average Filtering Method.* When there is the influence of large pulse interference, only using the average filtering method will average the larger pulse error into the filtering result, which will distort the filtered data [26]. The limited moving average filtering method can remove random large-scale interference on the basis of ensuring the smoothness of the processed data and make the filtered data highly fit the authenticity of the original data [27].

### 2.3. PI Algorithm for Speed Control System.

The PI algorithm is the most commonly used control algorithm applied to the speed control system. It is composed of two parts: the proportional regulator P and the integral regulator I [28]. The speed control system needs a fast and stable control effect, so the regulator P plays a role of rapid adjustment, and the integral regulator I plays a role of steady-state error-free, thus meeting the fast and stable requirements of the speed control system [29].

The PI regulator expression is

$$u(t) = k_p \left( \text{error}(t) + \frac{1}{T_1} \int_0^t \text{error}(t) \mathrm{d}t \right). \qquad (10)$$

Discrete processing is carried out:

$$u(k) = K_p \times \text{error}(k) + K_I \times \sum_{i=1}^{k} \text{error}(i). \qquad (11)$$

The incremental expression of the digital PI regulator is

$$\Delta u(k) = K_p \times [\text{error}(k) - \text{error}(k-1)] + K_I \times \text{error}(k). \qquad (12)$$

Incremental PI uses the deviation between the current error and the last error to obtain the output increment, so that there will be no cumulative error problem. The output formula is

$$u(k) = u(k-1) + \Delta u(k). \qquad (13)$$

The method part of this paper uses the abovementioned method to study the robotic arm control system based on AI

wearable acceleration sensor. The specific process is shown in Figure 1.

## 3. Experiment of Robotic Arm Control System Based on AI Wearable Acceleration Sensor

### 3.1. Structure Design of Test Platform Control System

#### 3.1.1. Servo Control System Component Design

*(1) Sensor Fixture.* Before designing the sensor fixture, we must first understand the sensor size and the structure of the indexing table disc. In order to facilitate the installation of 32 MEMS acceleration sensors on the VRNC-210 indexing table, corresponding sensor fixtures need to be designed. This project has designed an expansion disc and 32 L-shaped sensor fixtures to realize the installation of 32 sensors.

The expansion disc is connected to the VRNC-210 indexing table with M8 screws at 4 positioning holes, and the U-line card slot is designed according to the specific shape of the indexing table and 32 MEMS acceleration sensors of 20 mm × 20 mm × 20 mm. Then, use 3D CAD design software to model and design VRNC-210 indexing table, expansion disc, and L-shaped sensor fixture. Firstly, the model of VRNC-210 is established, and the model effect is that 32 L-shaped clamps are fixed on the expansion disk through 4 M2.5 screws, and the sensors are connected through 3 positioning holes at different positions on the L-shaped clamp, with a design diameter of 283 mm. The expansion disk can be placed at the same time to place 32 sensors to realize the static acceleration test of $X$, $Y$, and $Z$ axes.

*(2) Development of Interface Cables.* The entire test process must be carried out under standard environmental conditions, and a single temperature change can be maintained to record the impact of the external environment on the test results. The temperature performance test of the sensor needs to be carried out in the high- and low-temperature box. The acceleration sensor on the fixture is driven by the rotating shaft to operate in the high- and low-temperature box, and the temperature change in the high- and low-temperature box is set. Through continuous recording and analysis of the sensor in the set, different temperature
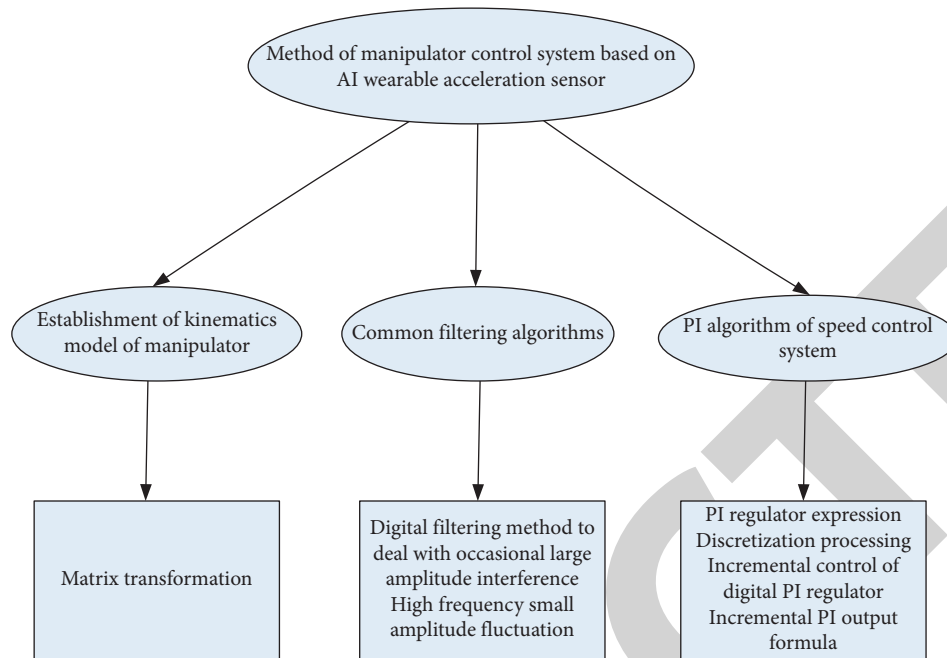
Figure 1: Part of the technical process of this method.

environments lower the output to get the relevant temperature performance index of the acceleration sensor. In the case of unexpected power failures in the servo control system, the motion control card must be combined with the RS-422 interface cable to ensure high-precision return to origin.

The high- and low-temperature box and the servo drive are respectively provided with RS-485 interface and RS-422 interface. First, the PCI slot of the industrial control computer can be installed with a model interface converter to expand a RS-485 and RS-422 hardware interface, respectively. General PCI interface conversion cards have built-in protection devices to suppress transient voltage to protect the transient overvoltage and surge voltage generated on the line for various reasons and use very small interelectrode capacitance to reliably ensure serial communication high-speed transmission.

### 3.1.2. Control Platform Collection Box

*(1) Shell Design of Data Acquisition Chassis.* Multichannel acquisition equipment needs to complete the acquisition of 32 analog channels and 32 digital channels. The acquisition equipment is mainly composed of analog signal acquisition subsystem, digital signal acquisition subsystem, power supply subsystem, and peripherals such as interfaces and indicators on the panel. The chassis is designed as a rectangular parallelepiped. In order to facilitate stacking with a 19-inch industrial computer (test control and data acquisition and processing computer), the width of the chassis is designed to be 429 mm.

*(2) Design of Power Supply Subsystem and Program-Controlled Power Supply.* Use Altium Designer 9.0 software to

complete the development of the power supply board. First, select the appropriate components in the component library of the software and place them in an accurate position. After naming them, set the packaging, etc., and use the components in the schematic area. The meaningful lines and symbols are connected to form a complete circuit schematic diagram. The schematic diagram should be easy to understand and clear. In order to prevent coupling during wiring, the input and output signal lines should be wired as much as possible, and the wires should be less bent, the width of the wires and the distance between the wires should be appropriately larger, and then you can design and generate the netlist to complete the error check and circuit modification to produce a qualified circuit board.

### 3.2. Cooperative Grasping Design of Wearable Robotic Arm.
The wearable robotic arm system designed in this research, wearable control gloves, can remotely grasp the identified objects, which has a good application prospect in production, life, industrial medical treatment, etc.

### 3.2.1. Collaborative Grabbing Action Design. 
In different scenes, facing different objects, the robotic arm can take different grasping actions to reduce the load of its steering gear and make the grasping objects more stable. Therefore, in view of the actual situation, this research carried out the registration of multiple actions on the robotic arm, so that the robotic arm can adapt to various situations. The entire grasping action is burned on the robotic arm control board through graphical software, so that the subsequent wearable control gloves can call the control information.

The software represents the six degrees of freedom of the robotic arm from different parts. Controlling different

freedoms to complete different actions can form a grasping action group. Adjust the PWM value of each degree of freedom to make the robotic arm complete different actions.

### 3.2.2. Glove Coordinated Control.

First, write the control program on the Arduino control board that controls the gloves, and then send the control commands to the actuator end of the robotic arm through the wireless communication module, so that the robotic arm executes different action groups to complete the grasping task. First, connect the control glove Arduino circuit board to the computer through the CH340 serial cable, then open the Arduino programming software, and select the corresponding development version model and COM port model; the port model here can be managed in the computer equipment after connecting the control glove to the computer. After setting the port number, you need to calibrate the wearable control gloves before entering the coordinated action.

Calibration requires two steps to complete: first, open the control glove upper computer software, which can realize data reception and data transmission. When the control glove is calibrated, its data receiving function is mainly used; then, wear the control glove and turn on the data glove ON button. If the indicator light is on, it is the working state. After pressing the calibration button on the circuit board, hold the five fingers and spread the five fingers in the opposite direction. Repeat this action several times to maximize the grip and stretch range of the ADXL345 tilt sensor. When subsequent commands for controlling the robotic arm are issued, different action groups can be accurately called for grabbing.

### 3.2.3. Judgment of the Suitability of the Object's Cooperative Grasping Temperature.

Sometimes, the temperature determination of the object to be grasped is also very important. Whether the temperature of the object is suitable for grasping is the problem to be solved. Under certain conditions, the temperature of the object to be grasped is too high or too low to damage the end jaws of the robotic arm. Therefore, judging the temperature of the object to be grasped is also a task to protect the wearable robotic arm system. In this study, a DS18B20 patch temperature sensor is placed at the end of a six-degree-of-freedom gripper to complete this task.

DS18B20 is a temperature sensor with a single bus interface. It only needs one I/O interface to communicate with the microprocessor, and it has the characteristics of small size, strong anti-interference ability, wide measurement range, and high accuracy. Its temperature measurement range is $-55°$ to $+125°$, and the accuracy is very high in the range of $-10°$ to $+85°$. In this study, a patch type DS18B20 sensor was used to solve the task, and the sensor module was encapsulated in a silicone wire.

Stick the DS18B20 probe on the sensitive area of the gripper end of the robotic arm to feel the temperature of the object being grasped. When the gripper at the end of the robotic arm grips the object, the patch temperature sensor DS18B20 will touch the temperature measurement object.

When the temperature of the object to be grasped exceeds $60°$, the temperature sensor transmits the signal to the STM32 single-chip microcomputer of the robot arm base, which is remotely transmitted to the control terminal through the wireless module. If there is a high temperature pop-up prompt, the operator should consider whether to continue grasping. If the grabbing temperature is normal, there is no other prompt, and the subsequent grabbing task can be performed.

### 3.2.4. Judgment of Pressure Threshold for Object Collaborative Grabbing.

Since the wearable robotic arm system grabs objects remotely, when the gripper of the actuator of the robotic arm grabs the object, it can be judged whether the grasped object is clamped according to the size of the force used. It is a remote control clamp. Take the key issues facing you. This research uses RFP602 chip piezoresistive pressure sensor and conversion module to solve this problem. Put the mechanical arm patch type piezoresistive pressure sensor on the jaw end of the actuator to solve the problem of measuring the pressure required to grasp different objects. When the external force acts on the sensing point, its resistance will become regular with the external force. When there is no pressure, the resistance value of the resistance is large and the maximum value. As the pressure value continues to increase, its resistance is continuously decreasing, which is inversely proportional to the pressure value. Connect the sensor to the voltage conversion module and connect it to the STM32 microcontroller to obtain the collected voltage. The pressure information is obtained through the resistance-pressure relationship conversion formula. Finally, the wireless module is fed back to the control terminal serial port, and the serial port feedback control end host.

This part of the experiment proposes the above-mentioned steps for the research experiment of the robotic arm control system based on the AI wearable acceleration sensor. The specific process is shown in Table 1.

## 4. Robotic Arm Control System Based on AI Wearable Acceleration Sensor

### 4.1. Experimental Correlation Analysis

(1) The first is the functional experiment of the gesture recognition manipulator. On the MEMS gesture sensing sensor, the hand makes a prescribed action, records the coordinate values related to the five gestures in processing, and observes whether the manipulator is set determined actions. In the process of gesture control, it is necessary to ensure that all dynamic actions should be within the designed working range, so that the steering gear can rotate in a matched manner. If the movement exceeds the range, the steering gear will lose the corresponding control. The data corresponding to different gesture controls are shown in Table 2 and Figure 2.

TABLE 1: Experimental steps in this article.

| | | | | |
|---|---|---|---|---|
| Research and experiment of manipulator control system based on AI wearable acceleration sensor | 3.1 | Structure design of test platform control system | 1 | Component design of servo control system |
| | | | 2 | Control platform collection box |
| | 3.2 | Cooperative grasping design of wearable manipulator | 1 | Cooperative grasping action design |
| | | | 2 | Cooperative control of gloves |
| | | | 3 | Determination of temperature suitability for object cooperative grasping |
| | | | 4 | Determination of pressure threshold for cooperative grasping of objects |

TABLE 2: Corresponding data of gesture control experiment.

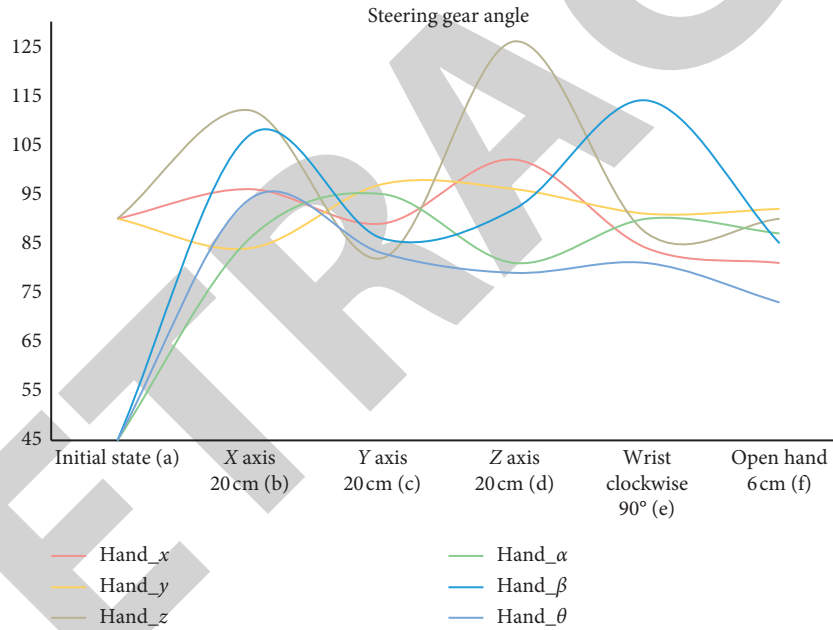| Steering gear angle (°) | hand_$x$ | hand_$y$ | hand_$z$ | hand_$\alpha$ | hand_$\beta$ | hand_$\theta$ |
|---|---|---|---|---|---|---|
| Initial state (a) | 90 | 90 | 90 | 45 | 45 | 45 |
| $X$ axis, 20 cm (b) | 96 | 84 | 112 | 86 | 107 | 94 |
| $Y$ Axis, 20 cm (c) | 89 | 97 | 82 | 95 | 86 | 83 |
| $Z$ axis, 20 cm (d) | 102 | 96 | 126 | 81 | 92 | 79 |
| Wrist clockwise, 90° (e) | 84 | 91 | 87 | 90 | 114 | 81 |
| Open hand, 6 cm (f) | 81 | 92 | 90 | 87 | 85 | 73 |



FIGURE 2: Corresponding data of gesture control experiment.

From the above experimental process and results, it can be seen that the functional verification experiments of dynamic gesture recognition and control of the five joints of the robotic arm can be successfully completed.

(2) This paper uses a two-segment rigid chain simulation model to verify the joint parameter estimation method based on joint constraints. A virtual measurement coordinate system is established at any position on the surface of rigid body A and rigid body B to simulate the measurement data of the inertial measurement unit. The rigid body A makes free rotation, and the rigid body B rotates around the rigid body A with two degrees of freedom. In order to verify the influence of linear acceleration measurement error on the estimation algorithm, noise was added to the signal. In the simulation data, 15 sets of data are randomly selected as the measurement data. When the system is noise-free, the estimated data are completely consistent with the preset parameters. The estimated error percentages of joint parameters under different linear acceleration measurement noises are shown in Table 3 and Figure 3.

It can be seen from the graph that when the linear acceleration measurement signal-to-noise ratio increases from 10 dB to 60 dB, the estimation error of the joint parameters drops from 5.37% to 0.81%.

TABLE 3: Error percentage of joint parameter estimation under different acceleration measurement noise.

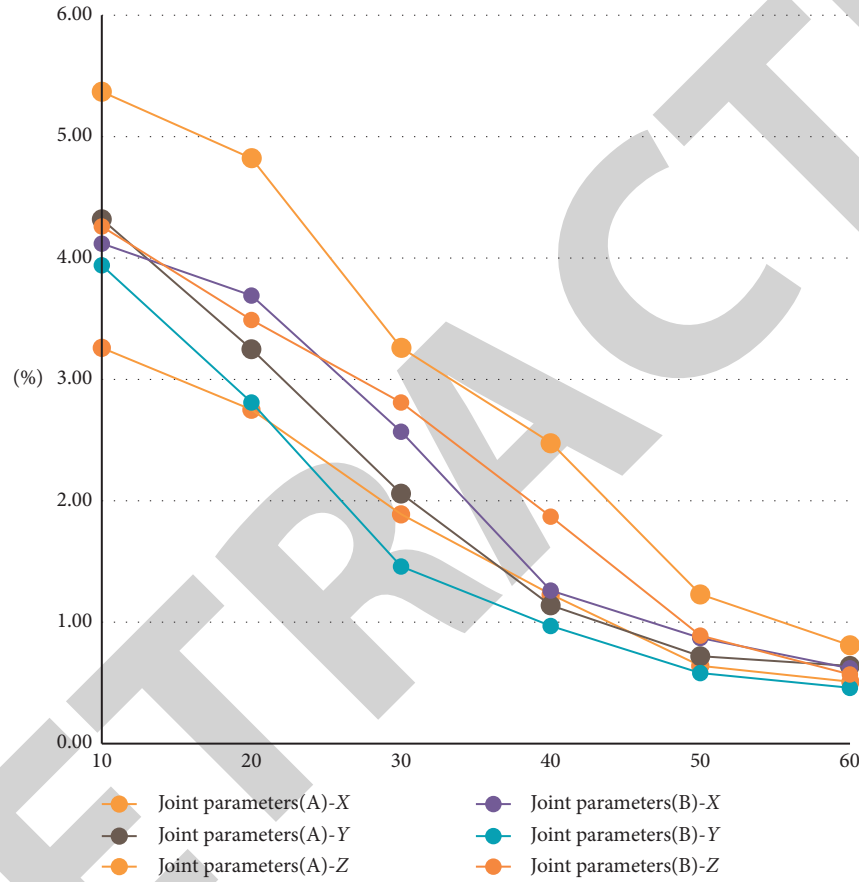| SNR (dB) | Joint parameters (A) | | | Joint parameters (B) | | |
|---|---|---|---|---|---|---|
| | X (%) | Y (%) | Z (%) | X (%) | Y (%) | Z (%) |
| 10 | 3.26 | 4.32 | 5.37 | 4.12 | 3.94 | 4.26 |
| 20 | 2.75 | 3.25 | 4.82 | 3.69 | 2.81 | 3.49 |
| 30 | 1.89 | 2.06 | 3.26 | 2.57 | 1.46 | 2.81 |
| 40 | 1.23 | 1.14 | 2.48 | 1.26 | 0.97 | 1.87 |
| 50 | 0.64 | 0.72 | 1.23 | 0.87 | 0.58 | 0.89 |
| 60 | 0.51 | 0.64 | 0.81 | 0.62 | 0.46 | 0.57 |



FIGURE 3: Error percentage of joint parameter estimation under different acceleration measurement noise.

## 4.2. System Performance Analysis

(1) When the system is running, the action feature as a representation has an obvious recognition effect in the JHMDB and MPII datasets. However, in the gesture sensing process, the complex background pixels affect the feature acquisition effect, thereby reducing the recognition efficiency, and 3D-SIFT is used. Representing static information improves the sensing effect. This paper selects the recognition rates of arms, elbows, wrists, and fingers to extract RGB features and SIFT features for comparison. The different feature recognition effects extracted from different body regions are shown in Table 4 and Figure 4.

From the recognition rates obtained by different methods, it can be seen that the action recognition

TABLE 4: Different feature recognition effects extracted from different arm regions.

| | RGB | SIFT |
|---|---|---|
| Arms | 8.9 | 10.4 |
| Elbows | 10.9 | 13.1 |
| Wrists | 11.3 | 12.6 |
| Fingers | 7.6 | 8.7 |

rate after using the elbow and wrist to propose features is relatively close. When the entire arm area is combined, the recognition rate is the highest, and compared with the direct recognition of the entire arm area, the recognition rate of the combination of various parts of the human body is the lowest.
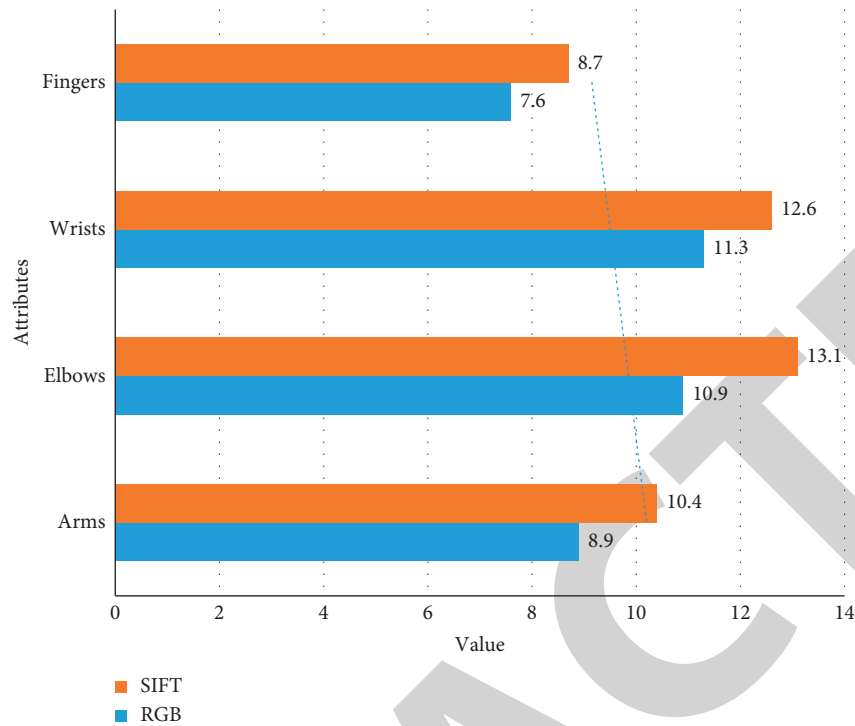
FIGURE 4: Different feature recognition effects extracted from different arm regions.

(2) The movement speed of different actions of the sports car body during the remote grasping task is also an index that cannot be ignored. By setting different values for PWM in the Arduino program, the rotation speed of the motor is different, but the PWM value is too high, the circuit current is large, and the burden on the circuit is also large, so in the test, set the PWM, PWM range is 0~255. In the open space in the laboratory, the speed of the vehicle body during various walking methods in omnidirectional motion was tested. The specific data are shown in Table 5 and Figure 5.

It can be seen from the abovementioned test data that the various speeds of the omnidirectional sports car body meet the actual requirements.

(3) In order to evaluate the proposed SIFT hardware architecture design, it is compared with other studies from the three perspectives of the stability of feature descriptors, the consumption of hardware resources, and the speed of hardware execution. Perform stability detection on the extracted feature descriptors, select an original image a, perform scale change, rotation, blur, and illumination on a to generate image b, and extract the feature descriptors of a and b for matching. The matching method is violent matching library functions provided by Opencv. Select 18 best matching point pairs from the

matching results. The matching rate is expressed by the ratio of the number of correct matching point pairs to 18. The higher the matching rate, the higher the stability of the feature descriptor. The results of the stability detection of the feature descriptor of the image rotating counterclockwise are shown in Table 6 and Figure 6.

From the calculation of the data in the chart, it can be concluded that the average matching rate after scale change processing is as high as 88.89%, and the feature descriptor stability is high. The rotated image feature descriptor is matched with the reference image feature descriptor. As the degree of rotation increases, the matching rate shows a downward trend.

(4) For the target recognition time, the system pure software target recognition time is about 10.81 seconds. The time for SIFT feature extraction is about 9.23 seconds. Draw the specific situation into a chart, as shown in Table 7 and Figure 7.

After using FPGA acceleration, the time for SIFT feature extraction is about 0.91 seconds, which is 8.32 seconds less than the pure software implementation. Therefore, after using FPGA acceleration, the target recognition time is reduced to 2.49 seconds, and the real-time performance is significantly improved.

Table 5: Movement speed test data.

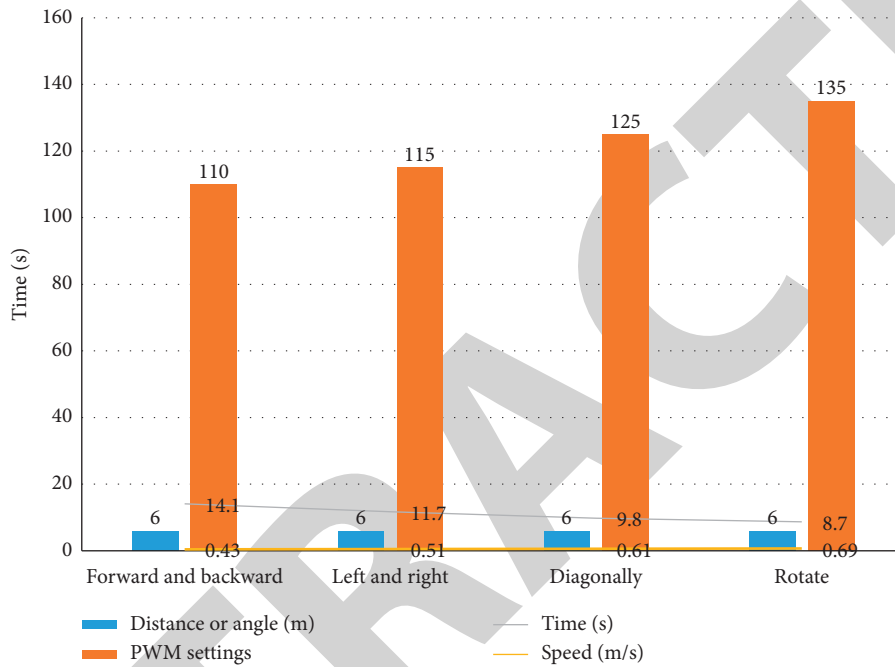| How to move | Distance or angle (m) | PWM settings | Time (s) | Speed (m/s) |
| --- | --- | --- | --- | --- |
| Forward and backward | 6 | 110 | 14.1 | 0.43 |
| Left and right | 6 | 115 | 11.7 | 0.51 |
| Diagonally | 6 | 125 | 9.8 | 0.61 |
| Rotate | 6 | 135 | 8.7 | 0.69 |



Figure 5: Movement speed test data.

Table 6: Rotation change feature descriptor stability detection.

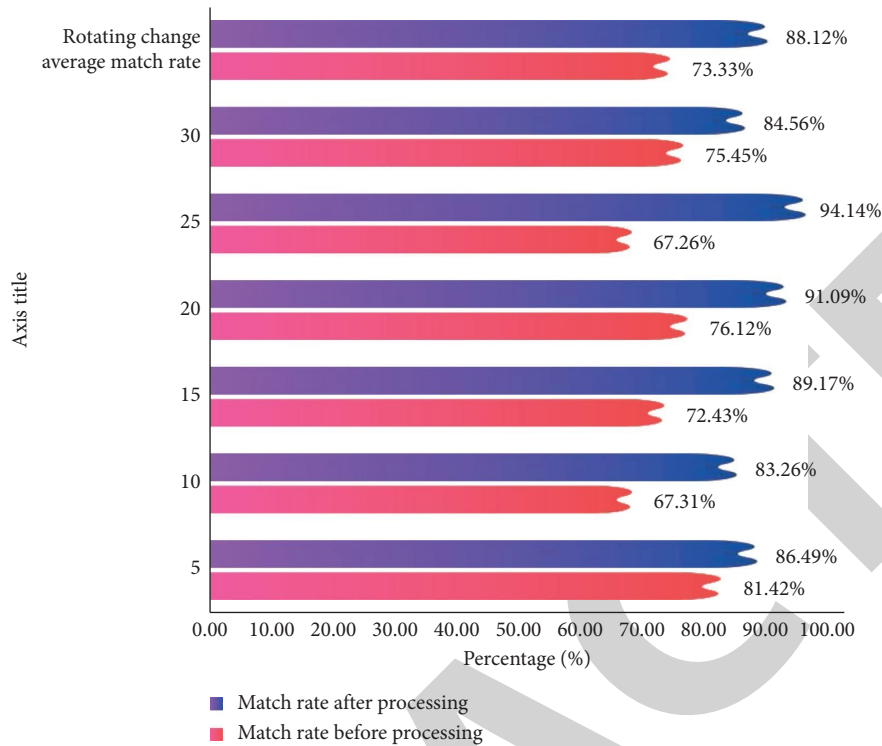| Degree of rotation (°) | Match rate before processing (%) | Match rate after processing (%) |
| --- | --- | --- |
| 5 | 81.42 | 86.49 |
| 10 | 67.31 | 83.26 |
| 15 | 72.43 | 89.17 |
| 20 | 76.12 | 91.09 |
| 25 | 67.26 | 94.14 |
| 30 | 75.45 | 84.56 |
| Rotating change average match rate | 73.33 | 88.12 |

FIGURE 6: Stability detection of rotation change feature descriptor.

TABLE 7: Comparison of target recognition time before and after acceleration.

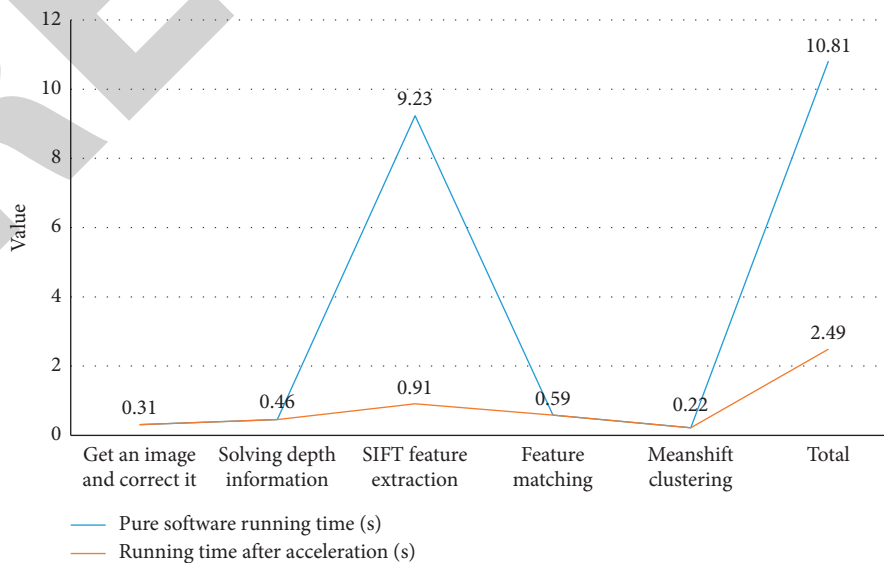| Target recognition | Pure software running time (s) | Running time after acceleration (s) |
| --- | --- | --- |
| Get an image and correct it | 0.31 | 0.31 |
| Solving depth information by stereo matching | 0.46 | 0.46 |
| SIFT feature extraction | 9.23 | 0.91 |
| Feature matching | 0.59 | 0.59 |
| Mean shift clustering | 0.22 | 0.22 |
| Total | 10.81 | 2.49 |



FIGURE 7: Comparison of target recognition time before and after acceleration.

## 5. Conclusions

With the development of computer technology, robotics technology has also matured. It combines technologies from computers, electronics, machinery, sensors, and control and is widely used in military, industry, agriculture, medicine, education, scientific research, and other fields. It basically covers all aspects of people's lives. As a powerful productivity tool, robots play a huge role in improving production efficiency, optimizing production methods, and broadening the production environment.

As a practical type of robot, the manipulator has extremely high work efficiency, stable repeatability, and powerful functions, so it is widely used in transportation services, product processing, and other fields. On the assembly line of high-tech manufacturing industry, various types of robotic arms can complete many different tasks, such as handling die-cast or stamped parts or components, laser cutting, and assembling mobile phone parts and painting them.

In this paper, the robot arm control system of the AI wearable acceleration sensor is designed to realize the remote grasping operation, which requires the whole body movement. The structure of the system is designed according to its functional requirements, and the main hardware is designed at the same time. First, select the model, aiming at the six-degree-of-freedom manipulator structure in this system, a sensor gesture recognition model is established based on the feature value extraction technology in the DH method; all software development environments used in this system are introduced in detail. In the design process of the robotic arm control system based on the AI wearable acceleration sensor, due to the limitations of experimental conditions and our professional level, there are still many shortcomings, such as the remote control distance being too short and the number of dynamic interactive gestures being insufficient. In the process of wireless data transmission, data security and anti-interference ability are not considered. This will be the focus and research direction of future work.

## Data Availability

No data were used to support this study.

## Conflicts of Interest

The authors declare that they have no conflicts of interest.

## References

[1]  M. H. Jarrahi, "Artificial intelligence and the future of work: human-AI symbiosis in organizational decision making," *Business Horizons*, vol. 61, no. 4, pp. 577–586, 2018.

[2]  D.-J. Choi and S.-J. Kang, "Software architecture of a wearable device to measure user's vital signal depending on the behavior recognition," *The Journal of Korean Institute of Communications and Information Sciences*, vol. 41, no. 3, pp. 347–358, 2016.

[3]  D. Navarro-Alarcon, H. M. Yip, Z. Wang et al., "Automatic 3-D manipulation of soft objects by robotic arms with an adaptive deformation model," *IEEE Transactions on Robotics*, vol. 32, no. 2, pp. 1–13, 2016.

[4]  D. Hassabis, D. Kumaran, C. Summerfield, and M. Botvinick, "Neuroscience-inspired artificial intelligence," *Neuron*, vol. 95, no. 2, pp. 245–258, 2017.

[5]  H. Lu, Y. Li, M. Chen et al., "Brain intelligence: go beyond artificial intelligence," *Mobile Networks and Applications*, vol. 23, no. 7553, pp. 368–375, 2017.

[6]  R. J. Spiro, B. C. Bruce, and W. F. Brewer, "Theoretical issues in reading comprehension: perspectives from cognitive psychology, linguistics, artificial intelligence, and education," *Reading Teacher*, vol. 3, pp. 368–373, 2017.

[7]  F.-Y. Wang, "Artificial intelligence and intelligent transportation: driving into the 3rd axial age with ITS," *IEEE Intelligent Transportation Systems Magazine*, vol. 9, no. 4, pp. 6–9, 2017.

[8]  N. N. Darren, Z. Alexey, S. Yasushi et al., "Synthetic biology routes to bio-artificial intelligence," *Essays in Biochemistry*, vol. 60, no. 4, pp. 381–391, 2016.

[9]  S. Jha and E. J. Topol, "Information and artificial intelligence," *Journal of the American College of Radiology*, vol. 15, no. 3, pp. 509–511, 2018.

[10]  A. Sarwar, J. Suri, M. Ali, and V. Sharma, "Novel benchmark database of digitized and calibrated cervical cells for artificial intelligence based screening of cervical cancer," *Journal of Ambient Intelligence & Humanized Computing*, vol. 12652, no. 16, pp. 353–358, 2016.

[11]  W. A. Marie, L. Yong, K. R. Regner et al., "Artificial intelligence, physiological genomics, and precision medicine," *Physiological Genomics*, vol. 50, no. 4, pp. 237–243, 2018.

[12]  D. Dai, "Human intelligence needs artificial intelligence," *Sensors*, vol. 5855, no. 3, pp. 95–99, 2018.

[13]  A. Bouzekri, T. Allaoui, M. Denai et al., "Artificial intelligence-based fault tolerant control strategy in wind turbine systems," *International Journal of Renewable Energy Research*, vol. 7, no. 2, pp. 652–659, 2017.

[14]  W. K. Lin, S. J. Lin, and T. N. Yang, "Integrated business prestige and artificial intelligence for corporate decision making in dynamic environments," *Cybernetics and Systems*, vol. 48, no. 4, pp. 1–22, 2017.

[15]  A. H. Yüzer, H. Sümbül, and K. Polat, "A novel wearable real-time sleep apnea detection system based on the acceleration sensor," *IRBM*, vol. 41, no. 1, pp. 39–47, 2020.

[16]  S. Lee, S. Gandla, M. Naqi et al., "All-day mobile healthcare monitoring system based on heterogeneous stretchable sensors for medical emergency," *IEEE Transactions on Industrial Electronics*, vol. 67, no. 10, pp. 8808–8816, 2020.

[17]  F. Tan, X. Xie, and L. Li, "Taekwondo motion state recognition system based on the wearable computing," *Journal of Mines Metals & Fuels*, vol. 65, no. 2, pp. 75–79, 2017.

[18]  M. Davide, B. Leonardo, C. Michele et al., "Profiling the propagation of error from PPG to HRV features in a wearable physiological-monitoring device," *Healthcare Technology Letters*, vol. 5, no. 2, pp. 59–64, 2018.

[19]  S. Li, P. Zhou, W. Xiao et al., "A wearable system for cervical spondylosis prevention based on artificial intelligence," *Zhongguo Yi Liao Qi Xie Za Zhi = Chinese Journal of Medical Instrumentation*, vol. 44, no. 1, pp. 33–37, 2020.

[20]  L. C. Wu, V. Nangia, K. Bui et al., "In vivo evaluation of wearable head impact sensors," *Annals of Biomedical Engineering*, vol. 44, no. 4, pp. 1234–1245, 2016.

[21] N. Dawar, S. Ostadabbas, and N. Kehtarnavaz, "Data augmentation in deep learning-based fusion of depth and inertial sensing for action recognition," *IEEE Sensors Letters*, vol. 3, no. 1, pp. 1–4, 2019.

[22] A. S. Jamaludin, M. N. Razali, N. Jasman, A. N. Ghafar, and M. A. Hadi, "Design of spline surface vacuum gripper for pick and place robotic arms," *Journal of Modern Manufacturing Systems and Technology*, vol. 4, no. 2, pp. 48–55, 2020.

[23] V. L. Nguyen, C. H. Kuo, and C. Y. Lin, "Gravity compensation design of planar articulated robotic arms using the gear-spring modules," *Journal of Mechanisms and Robotics*, vol. 12, no. 3, pp. 1–35, 2019.

[24] M. U. Farooq and S. Y. Ko, "An automated extracorporeal knot-tying system using two concentric tube robotic arms for deployment through a 3-mm port," *International Journal of Control, Automation and Systems*, vol. 18, no. 1, pp. 1–9, 2020.

[25] S. Wong and C. Gui, "Brain controlled robotic arms—advancements in prosthetic technology," *University of Western Ontario Medical Journal*, vol. 87, no. 2, pp. 59–61, 2019.

[26] M. Alikhani, B. Khalid, R. Shome, C. Mitash, K. Bekris, and M. Stone, "That and there: judging the intent of pointing actions with robotic arms," *Proceedings of the AAAI Conference on Artificial Intelligence*, vol. 34, no. 6, pp. 10343–10351, 2020.

[27] M. Falconi, "IEEE, control systems society, and women in engineering in Ecuador [member activities]," *IEEE Control Systems*, vol. 38, no. 4, pp. 15-16, 2018.

[28] L. Mönch, O. Rose, R. Sturm et al., "A simulation framework for the performance assessment of shop-floor control systems," *Simulation*, vol. 79, no. 3, pp. 163–170, 2003.

[29] Q. Li, J. Chen, N. P. Minton et al., "CRISPR-based genome editing and expression control systems in *Clostridium acetobutylicum* and *Clostridium beijerinckii*," *Biotechnology Journal*, vol. 11, no. 7, pp. 961–972, 2016.